CHALMERS
UNIVERSITY OF TECHNOLOGY

Public transport trajectory planning with probabilistic guarantees

Transportation Research Part B 139 (2020) 81–101

Contents lists available at ScienceDirect

Transportation Research Part B

journal homepage: www.elsevier.com/locate/trb

Public transport trajectory planning with probabilistic guarantees

Balázs Varga[a,*], Tamás Tettamanti[a], Balázs Kulcsár[b], Xiaobo Qu[c]

[a] Department of Control for Transportation and Vehicle Systems, Faculty of Transportation Engineering and Vehicle Engineering, Budapest University of Technology and Economics, Budapest, H-1111, Hungary
[b] Department of Electrical Engineering, Chalmers University of Technology, Gothenburg, SE-412-96, Sweden
[c] Department of Architecture and Civil Engineering, Chalmers University of Technology, Gothenburg, SE-412-96, Sweden

ARTICLE INFO

Article history:
Received 2 May 2019
Revised 14 April 2020
Accepted 12 June 2020

Keywords:
Eco-cruise control
Velocity control
Timetable reliability
Shockwave profile model
Chance-constrained optimization
Model predictive control

ABSTRACT

The paper proposes an eco-cruise control strategy for urban public transport buses. The aim of the velocity control is ensuring timetable adherence, while considering upstream queue lengths at traffic lights in a probabilistic way. The contribution of the paper is twofold. First, the shockwave profile model (SPM) is extended to capture the stochastic nature of traffic queue lengths. The model is adequate to describe frequent traffic state interruptions at signalized intersections. Based on the distribution function of stochastic traffic volume demand, the randomness in queue length, wave fronts, and vehicle numbers are derived. Then, an outlook is provided on its applicability as a full-scale urban traffic network model. Second, a shrinking horizon model predictive controller (MPC) is proposed for ensuring timetable reliability. The intention is to calculate optimal velocity commands based on the current position and desired arrival time of the bus while considering upcoming delays due to red signals and eventual queues. The above proposed stochastic traffic model is incorporated in a rolling horizon optimization via chance-constraining. In the optimization, probabilistic guarantees are formulated to minimize delay due to standstill in queues at signalized intersections. Optimization results are analyzed from two particular aspects, (i) feasibility and (ii) closed-loop performance point of views. The novel stochastic profile model is tested in a high fidelity traffic simulator context. Comparative simulation results show the viability and importance of stochastic bounds in urban trajectory design. The proposed algorithm yields smoother bus trajectories at an urban corridor, suggesting energy savings compared to benchmark control strategies.

1. Introduction

In busy urban arterials, particularly during peak hours delay of public transport is critical. Due to the stochastic nature of traffic networks, adherence to a bus schedule is not guaranteed. Fluctuation of passenger demand, intersection delays, changing traffic conditions and different driving styles of bus drivers bring several uncertainties into the system. Achieving

* Corresponding author.
E-mail addresses: varga.balazs@mail.bme.hu (B. Varga), tettamanti@mail.bme.hu (T. Tettamanti), kulcsar@chalmers.se (B. Kulcsár), xiaobo@chalmers.se (X. Qu).

https://doi.org/10.1016/j.trb.2020.06.005

List of symbols

ω	symbol of an elementary event
ρ_J	jam density
d ρ_C	critical density
$\rho_A(t, \omega)$	actual density
Q_C	peak capacity
$Q_A(t, \omega)$	arrival rate of vehicles, macroscopic vehicle flow
$F_{Q_A}(t, \varphi)$	CDF of the arrival rate $Q_A(t, \omega)$
φ	probability level
v_J	jam velocity
v_C	critical velocity
$v_A(t)$	free flow velocity of vehicles
l_q	tail of the queue
l_l	location of the traffic light
c	traffic light cycle counter
t_{cyc}	traffic light cycle time
t_1	start of the red traffic light phase
t_2	end of the red traffic light phase
t_{green}	green time interval
$W_1(t, \omega)$	queuing shockwave velocity
W_2	queue discharge wave velocity
$W_3(t, \omega)$	departure shockwave velocity
W_4	pressure wave
$R_J(t, \omega)$	queue traffic state
$R_C(t, \omega)$	queue discharge traffic state
$n(c, \omega)$	number of vehicles crossing the intersection at cycle c
$v(k)$	bus velocity at time step k
$x(k)$	bus position (relative to the start of the network) at time step k
Δt	discrete time step interval
τ	relaxation parameter
$v_{des}(k)$	desired velocity of the bus (control input)
$z_{tt}(k)$	timetable tracking error
$x_{tt}(k)$	timetable reference signal
t_0	time instant of the prediction
t_{ETA}	time of arrival of the bus to a stop
N	prediction horizon length
$J(k)$	optimization cost
$\underline{\underline{\mathcal{R}}}$	control input weighting matrix
$\underline{\underline{\mathcal{Q}}}$	tracking error weighting matrix
$\hat{R}_J(t, \omega)$	queue traffic state (spatially discretized)
$\hat{R}_C(t, \omega)$	queue discharge traffic state (spatially discretized)
$v_{\min}$	lower bound for the control input
$v_{\max}$	upper bound for the control input
ϵ	allowed position error at the bus stop
σ_{queue}	standard deviation of the queue length
$\sigma_{traj.}$	standard deviation of the predicted trajectories

timetable reliability in an environment where "traffic flow dynamics are dominated by external events (red traffic lights) rather than by the inherent traffic flow dynamics" (Papageorgiou, 1998) is especially difficult.

The need for increasing energy efficiency and the advances in driver assistance systems brought eco-cruise control strategies to life (Saerens et al., 2013), (Akhegaonkar et al., 2018), (Qu et al., 2020),. In rural areas the focus of eco-crusie control is on road topology (Hellström et al., 2010), (Németh and Gáspár, 2011). On the other hand, in urban areas interaction with traffic control devices dictate energy efficiency. The eCoMove project Vreeswijk et al. (2010) proposed a speed advisory system incorporating V2I communication with traffic lights. Simulation results suggested significant emission reduction. Kural et al. (2014) implemented a predictive traffic light assistant, that considers traffic light cycles during trajectory planning. However, they only considered traffic light cycles without queue lengths. Park et al. (2011) and Yang et al. (2017) constructed a dynamic programming based strategy to minimize fuel consumption in urban areas with traffic lights. The model

estimates queue lengths with the help of shockwaves. In Li et al. (2018) a trajectory smoothing algorithm was formulated considering platoons of connected automated vehicles and traffic lights.

Determining real-time queue length accurately at an intersection is difficult. Queue length is usually estimated from traffic flow data from loop detectors Sharma et al. (2007), video cameras Fathy and Siyal (1998) or various vehicle to infrastructure applications such as probe vehicles (Comert and Cetin, 2009). Several model based queue length approximation methods exist. Liu et al. (2009) estimated intersection queue length by using shockwave theory. The approach could estimate time-dependent queue length even when the signal links are congested with long queues. The main measures of performance at signalized intersections are the mean queue length and mean delay.

Previous authors tried to grasp the stochastic nature of traffic at signalized intersections. Darroch (1964) modeled queues at traffic lights as ergodic Markov chains. Heidemann (1994) dealt with statistical distribution of queue length at traffic signals and derived the probability generating functions of queue length and vehicle delays considering vehicle arrivals as Poisson process. In Mung et al. (1996) formulas are developed for the probability distributions of queue lengths at fixed time traffic signals. In Zheng et al. (2018) traffic flow states in an urban network with signalized intersections are estimated via stochastic Gaussian approximation.

As basis of this work, the traffic model called shockwave profile model (SPM) Wu and Liu (2011) is used to predict future traffic states upstream signalized intersections. In order to make up for possible simplification errors and overcome uncertainties and disturbances, this traffic model is augmented with stochastic assumptions: instead of using deterministic shockwave trajectories, shockwaves are represented with their probability density functions.

Parallel to trajectory control of individual vehicles, smart intersections and pre-signalizing strategies are also emerging with the increasing connectivity of urban transportation systems. Chow et al. (2017) aims at solving a similar timetable reliable bus control but with adjustable signal timing. Their approach is features a centralized, deterministic, computationally intensive algorithm. Whereas, we propose a decentralized, stochastic bus velocity control algorithm. In addition, it is possible to employ velocity control in conjunction with smart signalization.

According to Yang et al. (2016) it is beneficial to control connected automated vehicles and smart signal heads simultaneously, considering different automation levels. Guler and Menendez (2014) evaluates the effect of bus pre-signalizing in a mixed traffic environment. Although smart signal heads and dedicated bus lanes can significantly improve timetable reliability, city infrastructure often limits the implementation of such strategies. Klumpenhouwer and Wirasinghe (2018) proposed a bus holding strategy with Markov chains to model uncertainties arising during a bus trip. A dynamic bus holding strategy is proposed by Sánchez-Martínez et al. (2016). According to Daganzo (2009) a velocity control is more desirable than slack times or holding, since those are unproductive allocation of time in the cycle time of buses resulting in queuing at stops. Slack times can be dynamically addressed via changing the speed of the vehicle rather than holding it. In that sense, we propose a smoothed and pro-active way of slack time reduction foreseeing the trajectory to track. In the paper we aim at predicting an optimal trajectory for an urban bus, considering traffic light phases as input to the system, in order to enhance its timetable reliability (Saif et al., 2019).

There is only a small field for velocity control action possible: (i) in front of signalized intersections vehicle speed is entirely determined by the current phase of traffic (i.e. queuing, discharge) and (ii) delaying (slowing down) a vehicle in the course of the journey would only propagate the delay to other participants in traffic. Therefore, velocity control is only desirable when the controlled vehicle is further away from the intersection and traffic is not too dense or there is space for overtaking (e.g. multiple lanes, Gu et al. (2013)). The above assumption also suggests that the proposed bus velocity control does not perturb the trajectories of other participants of traffic significantly, thus the macroscopic characteristics and stochasticity of urban traffic flow are unaffected.

The contribution of this paper is twofold. First, the SPM model is introduced and augmented with the probabilistic nature of vehicle arrivals yielding a stochastic process. Second, a receding horizon model predictive velocity control is outlined for public transport buses. The ego-centric controller aims enhancing the timetable reliability of the controlled bus while predicting smooth, energy-efficient trajectory along a signalized arterial. The major contribution is considering traffic queue lengths via the stochastic SPM in the optimization as constraints, resulting in a chance-constrained MPC. Compared to Varga et al. (2018), surrounding traffic is considered in a more sophisticated way via the proposed stochastic approach. The calculated velocity from the controller can be used as reference for a cruise control system, or in a speed advisory function for the human driver, depending on the automation level of buses.

The paper is organized as follows. In Section 2 the stochastic shockwave profile model is introduced in three steps.

i) The model is formulated with probabilistic assumptions,
ii) the distribution of the queue length is derived as a stochastic process, and
iii) the proposed model is validated against a microscopic traffic simulator.

In Section 3 the predictive timetable tracking bus dynamics model is formulated. Section 4 merges the results of Section 2 and Section 3 and presents the cost function for the chance-constrained optimization. Feasibility analysis for the chance-constrained optimization is given in Section 5. Then, the performance of the controller is evaluated in a microscopic traffic simulation, compared to different benchmark control strategies. Finally, Section 6 concludes the findings of the paper.

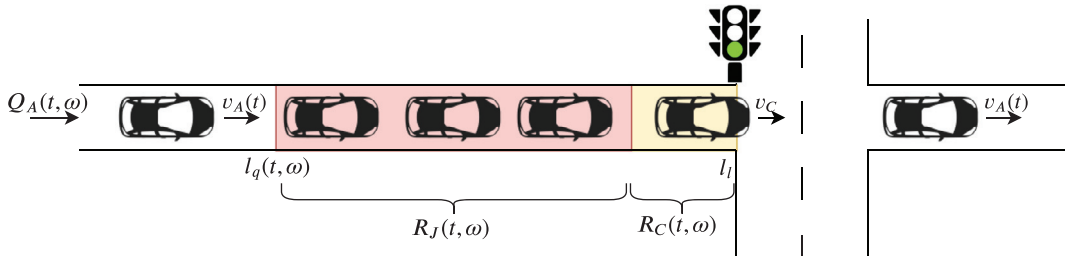

Fig. 1. Traffic flow states in front of a signalized intersection.

2. Stochastic shockwave profile model

This section presents the shockwave profile model and gives its stochastic extension. Stochasticity is injected into the model through the randomness of traffic flow. The model is discretized using passenger car equivalents (PCE). A simulation example is given to demonstrate the effectiveness of the model.

2.1. Stochastic queuing model

The deterministic SPM model, described in Wu and Liu (2011) is efficient in modeling networks with signalized intersections, where signal cycles and shockwaves shape traffic flow. The model distinguishes three different traffic states.

i) Traffic flows freely upstream the queue at the intersection, vehicles travel at their desired speed $v_A(t)$ $[\frac{m}{s}]$ and slow down when they approach the queue.
ii) Traffic is jammed inside, assuming jam density ρ_J and zero velocity $v_J = 0$. This traffic state is denoted by $R_J(t, \omega)$.
iii) When the queue starts dissipating, the traffic flow state goes from jammed to its critical capacity. The model calls this state queue discharge region $R_C(t, \omega)$. Here, the traffic flow is assumed to be saturated, the average velocity of vehicles is the critical velocity v_C.

The symbol $\omega \in \Omega$, introduced in $R_J(t, \omega)$ and $R_C(t, \omega)$ denotes one realization of the stochastic process. The probability space is defined as $[\Omega, \mathcal{A}, \mathbb{P}]$, where Ω is the sample space, $\mathcal{A}$ is a σ-algebra and $\mathbb{P}$ is the probability measure. The three regions of the model are depicted in Fig. 1. The tail of the queue $l_q(t, \omega)$ is marked by shockwave profiles.

As a contribution of the paper the SPM (Wu and Liu, 2011) is extended with the probabilistic nature of vehicle arrivals. Stochasticity is injected into the model through the following assumptions.

Assumption 1. Arrival rate distribution function The mean traffic inflow to the intersection, which is feeding the queue is assumed to be known (from real-time measurement or historical data (Daganzo and Lehe, 2016)): $\mathcal{Q}_A(t) = E[Q_A(t, \omega)]$ with known cumulative distribution function (CDF) $F_{Q_A}(t, \varphi) = \mathbb{P}(\omega : Q_A(t, \omega) \leq \varphi)$. In addition, the distribution function is truncated at zero flow and at peak capacity flow. When vehicles arrive from a link without traffic light or any obstacle that would perturb their distribution of arrivals, Poisson or Binomial process can be assumed (Heidemann, 1994), (Mung et al., 1996), with arrival rate $\mathcal{Q}_A(t)$. Otherwise, arrivals have generic truncated or discontinuous distributions. In addition, arrival rates may not be independent from traffic flow on the preceding links. Although, the model can give a probabilistic measure for queue spillover, it is assumed it does not occur. For brevity, in this paper, simple, independent distributions are used. This assumption can be relaxed with the considerations introduced in Appendix A.

Assumption 2. Ergodicity This assumption is the continuation of Assumption 1. In traffic engineering practice, traffic flow $\mathcal{Q}_A(t)$ is usually given in vehicles per hour, i.e. traffic signal program is planned based on hourly average traffic demand, usually determined from historical traffic data. However, a traffic light cycle time is only a fraction of an hour, i.e. more frequent sampling is needed. The hourly averaged traffic flow $\mathcal{Q}_A(t)$ and the cycle averaged traffic flow are not necessarily proportional, ergodicity of the traffic flow cannot be assumed. For example, 600 veh/h inflow and 60 s traffic light cycle does not mean that exactly 10 veh arrives in each cycle). This uncertainty is grasped through the distribution function of $Q_A(t, \omega)$ $(F_{Q_A}(t, \varphi))$.

Assumption 3. Fundamental diagram It is further assumed, that the link fundamental diagram (FD) is known in mean value. In the paper it is assumed to be measured (Chiabaut et al., 2009), (Qu et al., 2015) (Daganzo and Lehe, 2016), (Qu et al., 2017), (Seo et al., 2019). The link fundamental diagram describes the relation between the traffic flow states in a mixed traffic environment where the controlled buses operate. The purpose of the link FD in this work is to describe the traffic environment where the bus velocity control takes place. It is assumed that the network layout is such (e.g. multiple lanes, pull-in bus stops) and the frequency of the buses is so low that the repercussion of buses to the link FD is minor (Dakic et al., 2019). In addition, the bottleneck effect of the bus is minor if it is not significantly slower than the other vehicles and the traffic density is not extremely high and can be overtaken (Muñoz and Daganzo, 2002). In addition, the purpose of the queuing model is to be included into a predictive framework, where it is used to estimate queue lengths ahead the controlled bus. Vehicles downstream the bus shouldn't be affected by the bottleneck effect of the bus. For the

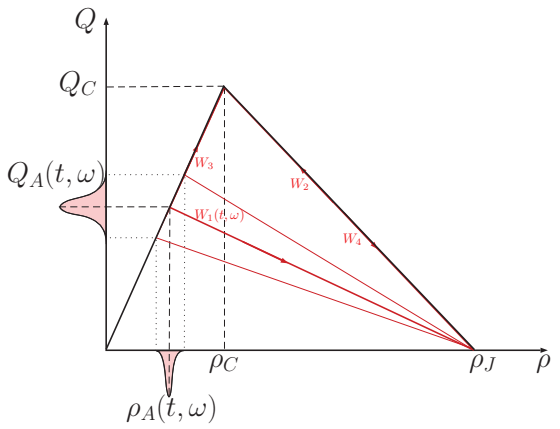

Fig. 2. Triangular link fundamental diagram of traffic flow with shockwaves. $Q_A(t, \omega)$ is represented with a probability density function, showing how it affects the slope of the queuing shockwave $W_1(t, \omega)$.

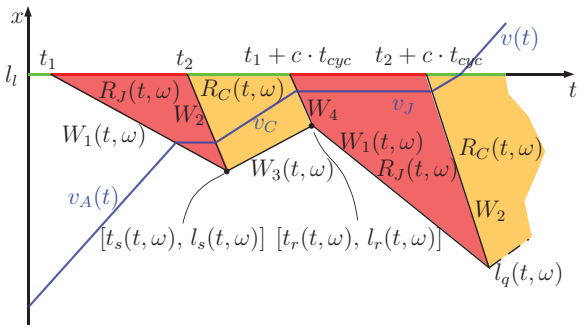

Fig. 3. Shockwave profile of a single intersection.

sake of simplicity, triangular link fundamental diagram is chosen (Laval and Castrillón, 2015). With the help of the specific points of the fundamental diagram (i.e. actual flow $[\rho_A(t, \omega), Q_A(t, \omega)]$, peak capacity $[\rho_C, Q_C]$ and jam density $[\rho_J, 0]$) the shockwave velocities $W_i(t, \omega)[\frac{m}{s}]\ i = 1 \dots 4$ can be computed analytically, see Fig. 2. It is further assumed, that the traffic flow is constant for short time intervals. The time-independent $Q_A(\omega)$ implies linear shockwave profiles.

Assumption 4. Signal program It is assumed, that the location of the traffic light $l_l[m]$ and the signal program are known. The signal program is represented by three variables: $t_{cyc}[s]$ is the cycle time, $t_{1,c}[s]$ is the start of red phase and $t_{2,c}[s]$ is the end of red phase in the cycle. Subscript c denotes the c^{th} traffic light cycle. The interrelation of the variables is as follows: the red time is $t_{red,c} = t_{2,c} - t_{1,c}$ and the green time is $t_{green,c} = t_{cyc,c} - t_{red,c}$. Therefore, $t_{cyc,c} = t_{red,c} + t_{green,c}$.

The model is capable of handling traffic responsive signal control too. There is a limitation though. The signal program shall be frozen for the MPC prediction horizon. If the signal program changes drastically during this horizon, it can bias the proposed velocity control algorithm. For brevity, the deductions and simulations in this paper employ static timing.

2.2. Shockwaves at signalized intersections

With the assumptions made in Section 2.1, herewith, we describe the effect of randomness in the SPM. The model distinguishes four shockwaves, depicted both in the link fundamental diagram (Fig. 2) and time-space diagram (Fig. 3). **Queuing shockwave velocity, $W_1(t, \omega)$** is formed by vehicles accumulating at the red light. Vehicles stopping at the tail of the queue from their actual velocity to zero form a shockwave. This process is also stochastic due to the randomness of vehicle arrivals affecting the queue length.

$$W_1(t, \omega) = -\frac{Q_A(t, \omega)}{\rho_J - \rho_A(t, \omega)}. \tag{1}$$

Discharge shockwave velocity, W_2 is assumed to be deterministic, as it is not affected by vehicle arrivals. In the fundamental diagram the discharge shockwave velocity is the slope of the line connecting the jam density and the critical density.

$$W_2 = -\frac{Q_C}{\rho_J - \rho_C}. \tag{2}$$

Table 1
Boundaries of traffic states.

Jam region ($R_J(t, \omega)$)	
Stop line during red (between $t_{1,c} + ct_{cyc}$ and $t_{2,c} + ct_{cyc}$)	l_l
Pressure wave (if exists)	$l_l + W_4(t - (t_{1,c} + ct_{cyc}))$
Queuing wave	$l_{r,c-1}(t, \omega) + W_1(t, \omega)(t - t_{r,c-1}(t, \omega))$
Discharge wave	$l_l + W_2(t - (t_{2,c} + ct_{cyc}))$
Discharge region ($R_C(t, \omega)$)	
Stop line during green (between $t_{2,c} + ct_{cyc}$ and $min(t_1 + ct_{cyc}, t_{r,c}(t, \omega))$)	l_l
Discharge wave	$l_l + W_2(t - (t_2 + ct_{cyc}))$
Departure wave	$l_{s,c}(t, \omega) + W_3(t, \omega)(t - t_{s,c}(t, \omega))$
Pressure wave (if exists)	$l_l + W_4(t - (t_1 + ct_{cyc}))$

Departure wave velocity $W_3(t, \omega)$ is generated as the queue dissipates as vehicles leave the intersection at green. It starts at the intersection of the queuing and discharge shockwaves. In addition, newly arrived vehicles feed the queue hence

$$W_3(t, \omega) = \frac{Q_C - Q_A(t, \omega)}{\rho_C - \rho_A(t, \omega)}. \tag{3}$$

Assuming a triangular link FD, the departure wave velocity becomes deterministic, see Fig. 2.

Pressure wave velocity W_4 separates a critical density and a jam density region, and it has the same speed as the discharge wave W_2. The pressure wave is only present if there is a residual queue, i.e. the queue cannot fully discharge during a green interval

$$W_4 = -\frac{Q_C}{\rho_J - \rho_C}. \tag{4}$$

Shockwave velocities can be represented in time-space diagram too, see Fig. 3. Shockwave profiles represent the building and dissipating of queues upstream a signalized intersection. The geometrical intersection point of the queuing and discharge shockwaves is the point $[t_{s,c}(t, \omega), l_{s,c}(t, \omega)]$. In addition, $t_{r,c}(t, \omega)$ is the time instant when the queue starts growing again in the next green phase. The residual queue length is $l_{r,c}(t, \omega)$. The shockwave intersection points $[t_{s,c}(t, \omega), l_{s,c}(t, \omega)]$ and $[t_{r,c}(t, \omega), l_{r,c}(t, \omega)]$ can be given analytically for c traffic light cycles ahead as:

$$t_{s,c}(t, \omega) = \frac{-W_1(t, \omega)t_{r,c-1}(t, \omega) + W_2(t_{2,c} + ct_{cyc}) + l_{r,c-1}(t, \omega) - l_l}{W_2 - W_1(t, \omega)}, \tag{5}$$

$$l_{s,c}(t, \omega) = W_1(t, \omega)(t_{s,c}(t, \omega) - t_{r,c-1}(t, \omega)) + l_{r,c-1}(t, \omega), \tag{6}$$

$$t_{r,c}(t, \omega) = min\left(t_{1,c} + ct_{cyc},\ \frac{-W_3(t, \omega)t_{s,c}(t, \omega) + W_4(t_{1,c} + ct_{cyc}) + l_{s,c}(t, \omega) - l_l}{W_4 - W_3(t, \omega)}\right), \tag{7}$$

$$l_{r,c}(t, \omega) = min(l_l,\ W_3(t, \omega)(t_{r,c}(t, \omega) - t_{s,c}(t, \omega)) + l_{s,c}(t, \omega)). \tag{8}$$

The discontinuities with $min(\ \cdot\ )$ are introduced to limit shockwaves upstream the intersection l_l. For brevity, ct_{cyc} is used to denote the time elapsed since an arbitrary initial time instant. In case of varying cycle lengths the notation modifies to $\Sigma_c t_{cyc,c}$.

In Fig. 3, the blue line depicts a vehicle trajectory with its velocity at each traffic phase, based on the SPM model. Upstream the intersection the vehicle travels freely at its desired velocity $v_A(t)$. When it enters the queue it stops, the jam velocity $v_J = 0$. In queue discharge vehicles assumed to travel with the equilibrium velocity at the critical density v_C.

To summarize, the space-time evolution of traffic phases in the SPM model can be given using the shockwave equations presented above for c traffic cycles ahead, where the number of elapsed cycles is

$$c = floor\left(\frac{t}{t_{cyc}}\right). \tag{9}$$

The regions in Fig. 3 can be described with the help of polygons made up of lines (assuming time independent vehicle inflow). The boundaries of $R_J(t, \omega)$ and $R_C(t, \omega)$ are summarized (for the c^{th} cycle) in Table 1. These boundaries will be used for introducing chance-constraints into the trajectory planning.

Outside these regions, vehicles travel at their desired speeds $v_A(t)$. The stochastic process for the queue length is:

$$l_q(t, \omega) = \begin{cases} W_1(t, \omega)(t - t_{r,c-1}(t, \omega)) + l_{r,c-1}(t, \omega), \\ if\ t_{r,c-1}(t, \omega) \le t < t_{s,c}(t, \omega)\ (queuing), \\ max(l_l, W_3(t, \omega)(t - t_{s,c}(t, \omega)) + l_{s,c}(t, \omega)), \\ if\ t_{s,c}(t, \omega) \le t < t_{r,c}(t, \omega)\ (departure). \end{cases} \tag{10}$$

2.3. Number of vehicles

To be able to compare the SPM to other urban traffic flow models, the number of vehicles (in passenger car equivalents, PCE) crossing the intersection in every cycle $n(c, \omega)$ shall be determined. The number of arriving vehicles per cycle is proportional to the slope of the arrival shockwave:

$$n_a(c,\omega) = \frac{W_1(t,\omega)t_{cyc}}{l_{PCE} + l_{jam}}. \tag{11}$$

The number of outflowing vehicles in cycle c is proportional to the decrement of queue length in the green phase $l_{s,c}(\omega)$. In mathematical form:

$$n_d(\omega) = min\left(\frac{W_2 t_{green}}{l_{PCE} + l_{crit}},\ n(c,\omega) + \frac{W_1(t,\omega)t_{cyc}}{l_{PCE} + l_{jam}}\right), \tag{12}$$

where l_{PCE} is the PCE length, l_{crit} is the average headway distance at the critical density (which is assumed to prevail in the queue discharge region). l_{jam} is the headway distance in jam. The green time interval is $t_{green} = t_{cyc} - (t_2 - t_1)$. $n(c, \omega)$ denotes the number of vehicles in traffic light cycle c. In the same vein, the queue length evolution (in PCE) over one cycle c can be given as:

$$n(c+1,\omega) = n(c,\omega) + n_a(c,\omega) - n_d(c,\omega), \tag{13}$$

within time period $[ct_{cyc}, (c+1)t_{cyc}]$. This result in Eq. (13) is a discrete-time traffic model, similar to the store-and-forward model (Aboudolas et al., 2009), however the shockwave profile model is capable of handling undersaturated networks too. Furthermore, this formula is needed to extend the SPM to multiple links, see Appendix A.

2.4. CDF Of shockwaves

Next, the stochastic shockwave profiles and their respective cumulative density functions (CDFs) are derived analytically. First, the relationship of the CDFs of traffic flow $F_{Q_A}(t,\varphi)$ and traffic density $F_{\rho_A}(t,\varphi)$ is derived, using Theorem 1.

Theorem 1. *Let $\xi(\omega)$ be a random variable with CDF $F_\xi(\varphi)$. Let $\eta(\omega) = g(\xi(\omega))$. The CDF of $\eta(\omega)$ can be given as:*

$$F_\eta(\varphi) = \begin{cases} F_\xi(g^{-1}(\varphi)), & if\ g(\varphi)\ is\ monotonically\ increasing, \\ 1 - F_\xi(g^{-1}(\varphi)), & if\ g(\varphi)\ is\ monotonically\ decreasing, \end{cases} \tag{14}$$

and if $g(x)$ has a unique inverse (Arnold, 2013).

Now, let's analyze the relationship of the CDFs of traffic flow and traffic density.

Given the vehicle arrivals $Q_A(t, \omega)$ and assuming mean-valued triangular link fundamental diagram (Eq. (15)), the traffic density $\rho_A(t, \omega)$ in the uncongested region can be determined:

$$\rho_A(t,\omega) = \frac{1}{v_f} \cdot Q_A(t,\omega), \tag{15}$$

assuming free flow at the beginning of the link, with v_f being the velocity at free flow. In addition, the distribution of $Q_A(t, \omega)$ has to be truncated from both sides: it has to be greater than zero and smaller than Q_C. $F_{\rho_A}(t,\varphi)$ in the free flow region is given as:

$$F_{\rho_A}(t,\varphi) = F_{Q_A}(t, g^{-1}(\varphi)), \tag{16}$$

with $g(x)$ being the relation in Eq. (15). Therefore:

$$F_{\rho_A}(t,\varphi) = F_{Q_A}(t, v_f \cdot \varphi). \tag{17}$$

The next step in formulating the stochastic traffic flow model to describe the CDFs of the shockwaves. In the model, only $W_1(t, \omega)$ and $W_3(t, \omega)$ depend on the random arrivals $Q_A(t, \omega)$ as:

$$W_1(t,\omega) = \frac{Q_J - Q_A(t,\omega)}{\rho_J - \rho_A(t,\omega)} = -\frac{Q_A(t,\omega)}{\rho_J - \frac{1}{v_f}Q_A(t,\omega)}. \tag{18}$$

$$W_3(t,\omega) = \frac{Q_C - Q_A(t,\omega)}{\rho_C - \rho_A(t,\omega)} = \frac{Q_C - Q_A(t,\omega)}{\rho_C - \frac{1}{v_f}Q_A(t,\omega)}. \tag{19}$$

Since $F_{Q_A}(t,\varphi)$ is known, $F_{W_1}(t,\varphi)$ and $F_{W_3}(t,\varphi)$ can be formulated for the arrival and the departure wave velocities, respectively, with the help of Theorem 1 again. The $g^{-1}(\varphi)$ functions are the inverses of Eq. (18) and Eq. (19), with $Q_A(t,$

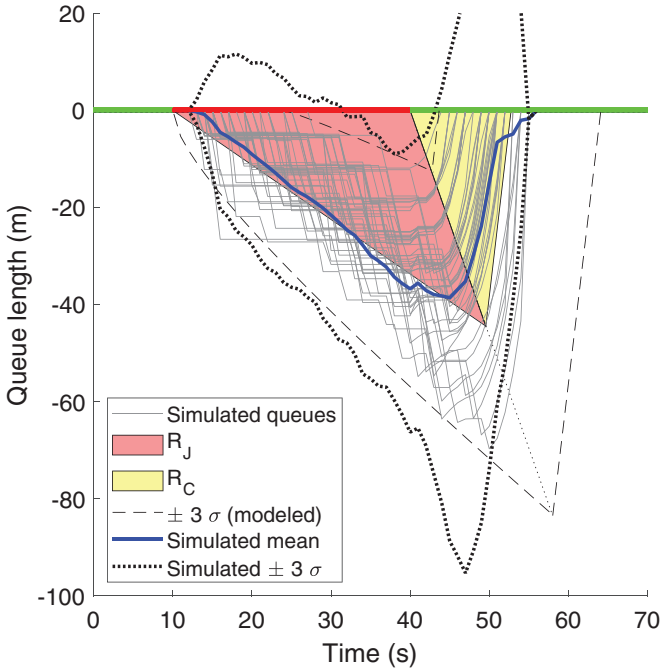

Fig. 4. Monte Carlo simulation of queue lengths.

ω) replaced by level φ. Note that in Eq. (18) $W_1(t, \omega)$ is a decreasing function of $Q_A(t, \omega)$. Likewise, $W_3(t, \omega)$ is increasing function of $Q_A(t, \omega)$. With this in mind, the resulting CDFs become:

$$F_{W_1}(t, \varphi) = 1 - F_{Q_A}\left(t, -\frac{\rho_J - \frac{1}{v_f}\varphi}{\varphi}\right), \tag{20}$$

$$F_{W_3}(t, \varphi) = F_{Q_A}\left(t, \frac{\rho_C - \frac{1}{v_f}\varphi}{\rho_C - \varphi}\right), \tag{21}$$

if $Q_A(t, \omega)$ is nonzero. Similarly, the CDF of the queue length $F_{l_q}(t, \varphi)$ as a stochastic process can be computed. When the expressions for the shockwave velocities and recursively calculated intersection points are substituted, the stochastic process of the queue length becomes only $Q_A(t, \omega)$ dependent. The relation between $Q_A(t, \omega)$ and $l_q(t, \omega)$ is a piecewise, truncated, first order rational function. With Theorem 1, $F_{l_q}(t, \varphi)$ can be computed even though the expression becomes very long and we omit it for brevity.

2.5. Example

This section demonstrates how the proposed traffic model is capable of capturing the stochastic nature of queue lengths at a traffic light. For simplicity, the arrival rate of vehicles is characterized by a homogeneous Poisson distribution with constant $\lambda = \mathcal{Q}_A = E[Q_A(\omega)]$ arrival rate.

Exploiting the linear property of the Poisson process, the arrival rate can be scaled down (e.g. $360\,veh/h \rightarrow 0.1\,veh/s$) and still have a Poisson process. Note: the resulting stochastic process is also a homogeneous Markov chain (Karlin, 1957). The shockwave model, however, is different from an $M/M/1$ service model. It also considers the temporal piecewise nature of traffic signal phases (i.e. red and green phases) and distinguishes queuing and discharge sequences.

Next, a numerical simulation example is given, in order to validate the proposed traffic model. A Monte Carlo simulation was run in a microscopic traffic simulator VISSIM (PTV, 2011). The simulation consisted of one link, ending with a traffic light at $300\,m$. The link fundamental diagram was assumed to be known. The fixed-time traffic light cycle time is $60\,s$ and the green time was set to 30s. Vehicles arrived at the traffic light with Poisson distribution with hourly rate $\lambda = 500\,veh/h$. The simulation was $15000\,s$ long, resulting 250 traffic light cycles. Queue lengths were logged and compared against the stochastic shockwave profile model. According to Fig. 4, the average queue length and standard deviations in the queuing phase were accurately estimated. The estimation error in the queuing phase was 5.6%. Standard deviations are overestimated when two traffic states co-exist in the queue. The slope of the dissipation wave was well estimated too with 7.1% error but the start of the dissipation phase was incorrectly modeled. The error stems from the randomness of vehicle arrivals and the modeling error of the assumed link fundamental diagram.

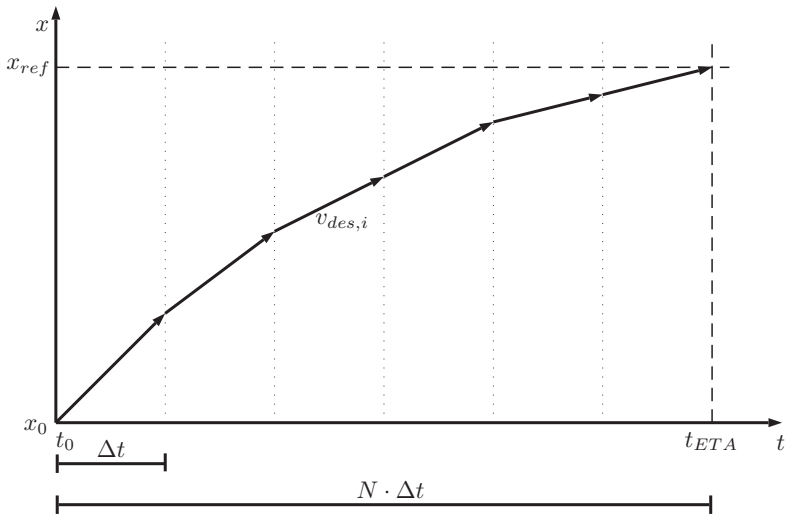

Fig. 5. MPC horizon length calculation.

3. Timetable tracking bus dynamics model

In this section, a bus dynamics model is formulated for control design purposes. Buses operate on a route in mixed traffic based on their timetable. When the schedule is tight, their trajectory shall be carefully planned. Hence, probabilistic constraints will be added by adopting the stochastic SPM introduced in Section 2.

The proposed bus velocity control algorithm (referred hereafter as control algorithm) creates an optimal trajectory within a predefined prediction horizon considering the schedule and red times at signalized intersections. The state-space representation of the discrete-time longitudinal dynamics of the bus is:

$$\overbrace{\begin{bmatrix} v(k+1) \\ x(k+1) \end{bmatrix}}^{X(k+1)} = \overbrace{\begin{bmatrix} 1-\frac{\Delta t}{\tau} & 0 \\ \Delta t & 1 \end{bmatrix}}^{A} \overbrace{\begin{bmatrix} v(k) \\ x(k) \end{bmatrix}}^{X(k)} + \overbrace{\begin{bmatrix} \frac{\Delta t}{\tau} \\ 0 \end{bmatrix}}^{B} v_{des}(k). \tag{22}$$

Discrete-time differential equation system Eq. (22) is evaluated under time period $[k,\ k+1]\Delta t$ where $k = 0,\ 1,\ 2,\ \ldots$ is the time step index and $\Delta t = 2\ s$ is the sampling interval. The system states of a bus are its velocity and position: $X(k) = [v(k), x(k)]^T$. τ is a relaxation parameter capturing the sensitivity of drivers' to the change of their desired velocity. According to Helbing and Tilch (1998) it shall be calibrated between 1.25 s and 2.5 s. Too small or high values would result in unrealistic accelerations or decelerations towards the desired velocity. The control input is the desired velocity $v_{des}(k)$. The controller calculates an optimal velocity profile v_{des} towards the subsequent bus stop, obeying constraints set by the timetable and queues at intersections. The calculated control input can serve as a display to the driver or a strict reference signal for autonomous driving to anticipate traffic states. Timetable tracking is incorporated into the model via an error term:

$$z_{tt}(k) = \overbrace{\begin{bmatrix} 0 & -1 \end{bmatrix}}^{C} \overbrace{\begin{bmatrix} v(k) \\ x(k) \end{bmatrix}}^{X(k)} + x_{tt}(k), \tag{23}$$

where $x_{tt}(k)$ is an idealized reference trajectory based on the timetable of the bus. The timetable is a set of points in the time-space diagram (i.e. the bus shall be at a given stop at a given time).

The control oriented model is used as basis of a shrinking horizon MPC (Maciejowski, 2002). The goal of the controller is calculating an optimal velocity profile between its actual position and the next stop. At each time step, the MPC technique: (i) predicts the traffic conditions along a future time window based on the system model; (ii) minimizes an a priori defined network-related performance index by finding the appropriate control input; and (iii) applies only the first optimal decision variable.

The shrinking horizon MPC prediction length depends on the scheduled travel time to the next bus stop. The interval between the time instant of the prediction (denoted by t_0) and the desired arrival time to the next stop (denoted by t_{ETA}, i.e. expected time of arrival is split into N equidistant steps, see Fig. 5. In every time step the prediction horizon decreases by one. By the last time step the bus shall arrive at the desired stop. To avoid small or even negative horizon lengths (due

to lateness or being close to the stop) a lower bound is introduced: $N_{\min} = 5$. That is:

$$N = max\left\{N_{min},\ \frac{t_{ETA} - t_0}{\Delta t}\right\}. \tag{24}$$

Consider the state space representation in Eq. (22) and tracking performances Eq. (23) and extend it for N horizon, see Eq. (25). The system state $X(k)$ is measured at time step k. Then, for a finite horizon length N the future states $X(k+i|k)$ are calculated along with the corresponding control input $v_{des}(k+i-1|k)$ and the external reference signal $x_{tt}(k+i-1|k)$. Predicted states are denoted as $X(k+i|k)$, where time step k at the right side within the parentheses denotes the current time, and $k+i$ at the left side the prediction step with running index $i = 1, 2, \ldots, N$. The same notation applies for the control input, the external signals and the performance output $z_{tt}(k+i|k)$, see Eqs. (25)-(26).

$$\overbrace{\begin{bmatrix} X(k+1|k) \\ X(k+2|k) \\ \vdots \\ X(k+N|k) \end{bmatrix}}^{\hat{\mathbf{x}}} = \overbrace{\begin{bmatrix} A \\ A^2 \\ \vdots \\ A^N \end{bmatrix}}^{\underline{\mathcal{A}}} \overbrace{X(k|k)}^{\mathbf{x}} + \overbrace{\begin{bmatrix} B & 0 & \cdots & 0 \\ AB & B & & 0 \\ \vdots & \vdots & \ddots & \vdots \\ A^{N-1}B & A^{N-2}B & \cdots & B \end{bmatrix}}^{\underline{\underline{\mathcal{B}}}} \overbrace{\begin{bmatrix} v_{des}(k|k) \\ v_{des}(k+1|k) \\ \vdots \\ v_{des}(k+N-1|k) \end{bmatrix}}^{\underline{\mathbf{u}}} \tag{25}$$

$$\overbrace{\begin{bmatrix} z_{tt}(k+1|k) \\ z_{tt}(k+2|k) \\ \vdots \\ z_{tt}(k+N|k) \end{bmatrix}}^{\hat{\mathbf{z}}_{tt}} = \overbrace{\begin{bmatrix} C & 0 & \cdots & 0 \\ 0 & C & & 0 \\ \vdots & \vdots & \ddots & \vdots \\ 0 & 0 & \cdots & C \end{bmatrix}}^{\underline{\underline{\mathcal{C}}}} \overbrace{\begin{bmatrix} X(k+1|k) \\ X(k+2|k) \\ \vdots \\ X(k+N|k) \end{bmatrix}}^{\hat{\mathbf{x}}} + \overbrace{\begin{bmatrix} 1 & 0 & \cdots & 0 \\ 0 & 1 & & 0 \\ \vdots & \vdots & \ddots & \vdots \\ 0 & 0 & \cdots & 1 \end{bmatrix}}^{\underline{\underline{\mathcal{D}}}} \overbrace{\begin{bmatrix} x_{tt}(k+1|k) \\ x_{tt}(k+2|k) \\ \vdots \\ x_{tt}(k+N|k) \end{bmatrix}}^{\hat{\sigma}_{tt}}. \tag{26}$$

4. Formulating the cost function

In order to formulate a real-time optimization problem with chance-constraints (probabilistic constraints) the results of Section 2 and 3 are merged. The optimization aims at solving a quadratic problem to control the velocity of individual buses in signalized arterials in a predictive manner.

4.1. Quadratic cost function

The cost function to be minimized in the optimization is sought in the following standard quadratic form:

$$J(k) = \frac{1}{2}\left[\hat{\mathbf{z}}_{tt}^T \underline{\underline{\mathcal{Q}}}\, \hat{\mathbf{z}}_{tt} + \underline{\mathbf{u}}^T \underline{\underline{\mathcal{R}}}\, \underline{\mathbf{u}}\right]. \tag{27}$$

$\hat{\mathbf{z}}_{tt}$ and $\underline{\mathbf{u}}$ denote stacked vectors of the predicted reference trajectory error and the control input (desired velocity) at every time iteration. $\underline{\underline{\mathcal{Q}}}^{N\times N}$ and $\underline{\underline{\mathcal{R}}}^{N\times N}$ are positive definite, diagonal weighting matrices. Each value in $\underline{\underline{\mathcal{Q}}}$ and $\underline{\underline{\mathcal{R}}}$ belongs to one time-step in the prediction. The higher values in $\underline{\underline{\mathcal{Q}}}$ means more emphasis on timetable tracking performance (i.e. the predicted trajectory shall mimic the reference). $\underline{\underline{\mathcal{R}}}$ penalizes the control input. Selecting too small values for $\underline{\underline{\mathcal{R}}}$ would result in saturated control signal and poor energy-efficiency. On the other hand, too high values in $\underline{\underline{\mathcal{R}}}$ yields slow response and the desired performance criteria (timetable adherence) might not be met. A quadratic formula means that it penalizes both positive and negative deviations from the reference (i.e. not only late but also early arrival).

By inserting Eq. (25) into Eq. (26), then the resulting expression into Eq. (27) and following some simple algebraic steps, the cost function simplifies to:

$$\begin{aligned} J(k) = &\frac{1}{2}\underline{\mathbf{u}}^T\left(\underline{\underline{\mathcal{B}}}^T\underline{\underline{\mathcal{C}}}^T\ \underline{\underline{\mathcal{Q}}}\,\underline{\underline{\mathcal{C}}}\,\underline{\underline{\mathcal{B}}} + \underline{\underline{\mathcal{R}}}\right)\underline{\mathbf{u}} \\ &+ \left(\mathbf{x}^T\underline{\underline{\mathcal{A}}}^T\underline{\underline{\mathcal{C}}}^T\ \underline{\underline{\mathcal{Q}}}\,\underline{\underline{\mathcal{C}}}\,\underline{\underline{\mathcal{B}}} + \hat{\sigma}^T\underline{\underline{\mathcal{D}}}^T\ \underline{\underline{\mathcal{Q}}}\,\underline{\underline{\mathcal{C}}}\,\underline{\underline{\mathcal{B}}}\right)\underline{\mathbf{u}} = \frac{1}{2}\underline{\mathbf{u}}^T\Phi\underline{\mathbf{u}} + \Omega^T\underline{\mathbf{u}}. \end{aligned} \tag{28}$$

For detailed deduction steps, please refer to Varga et al. (2018).

Next, optimization constraints are considered. It is assumed that the control input is constrained: the lower limit $v_{\min} = 0\ km/h$, since negative velocity is not allowed. The desired velocity has an upper bound too: it is either constrained by the legal speed limit on the link (e.g. $v_{lim} = 50\ km/h$) or if the link is congested, the bottleneck speed $v_{btl}(k)$ imposed by other vehicles: $v_{\max} = \min(v_{btl}(k),\ v_{lim})$. In the rolling horizon framework, the velocity bound is assumed to be constant within one horizon. The aim of the control algorithm is driving the vehicle to the next stop. It can be formulated with the help of two constraints. At the final prediction step the absolute tracking error $|z_{tt}(k+N|k)|$ shall be smaller than a threshold $\epsilon \approx 2\,m$ (e.i. it shall be at the bus stop). In addition, the bus shall come to a full stop there. Finally, the effect of traffic signal states is incorporated into the model as probabilistic constraints via the proposed stochastic shockwave profile model.

4.2. Chance-constraints

If the controlled bus is in the queue upstream a traffic light $R_J(t,\omega)$, it cannot move. If it is in the queue discharge $R_C(t,\omega)$, its velocity is constrained by the surrounding traffic. The stochastic nature of the regions $R_J(t,\omega)$ and $R_C(t,\omega)$ turns the optimization into a chance-constrained MPC (Campi et al., 2009). With the results in Table 1, the controlled bus being in either of the regions can be written:

$$x(k) \in R_J(t,\ \omega)\ if\ \begin{cases} x(k) < l_l, \\ x(k) > l_l + W_2(t-(t_2+ct_{cyc})), \\ x(k) < l_{s,c}(t_{s,c},\omega) + W_3(t,\omega)(t - t_{s,c}(t,\omega)), \\ x(k) > l_l + W_4(t-(t_1+(c+1)t_{cyc})). \end{cases} \tag{29}$$

Similarly,

$$x(k) \in R_C(t,\ \omega)\ if\ \begin{cases} x(k) < l_l, \\ x(k) > l_l + W_4(t-(t_1+ct_{cyc})), \\ x(k) > l_{r,c-1}(t_{r,c},\omega) + W_1(t,\omega)(t - t_{r,c-1}(t,\omega)), \\ x(k) < l_l + W_2(t-(t_2+ct_{cyc})), \end{cases} \tag{30}$$

with $k = floor\left(\frac{t}{\Delta t}\right)$ being the discrete time step. The discrete time MPC takes samples from the continuous time shockwave profile model. Note that stochasticity only arises in the third case which describes the tail of the queue in both Eq. (29) and Eq. (30), the other lines bounding the regions $R_J(t,\omega)$ and $R_C(t,\omega)$ are deterministic. This means that stochasticity is only involved in the actual length of the queue, which was already calculated in Section 2.

The conditional probability $\mathbb{P}(\cdot)$ of $x(k)$ being in $R_C(t,\omega)$ can be written as follows:

$$\begin{aligned} &\mathbb{P}\{\omega : x(k) \in R_C(t,\ \omega)\} \\ &= \mathbb{P}\{\{\omega : l_{r,c-1}(t_{r,c},\omega) + W_1(t - t_{r,c-1}(t,\omega)) > x(k)\} | \{x(k) < l_l\} \wedge \\ &\quad \wedge \{x(k) > l_l + W_4(t-(t_1+ct_{cyc}))\} \wedge \{x(k) < l_l + W_2(t-(t_2+ct_{cyc}))\}\}. \end{aligned} \tag{31}$$

Similarly,

$$\begin{aligned} &\mathbb{P}\{\omega : x(k) \in R_J(t,\ \omega)\} \\ &= \mathbb{P}\{\{\omega : l_{s,c}(t_{s,c}\omega) + W_3(t,\omega)(t - t_{s,c}(t,\omega)) > x(k)\} | \{x(k) < l_l\} \wedge \\ &\quad \wedge \{x(k) > l_l + W_2(t-(t_2+ct_{cyc}))\} \wedge \{x(k) > l_l + W_4(t-(t_1+(c+1)t_{cyc}))\}\}. \end{aligned} \tag{32}$$

The CDFs $F_{x(k)\in R_J(t,\ \omega)}(\varphi)$ and $F_{x(k)\in R_C(t,\ \omega)}(\varphi)$ for the probabilities of a point is within region $R_C(t,\omega)$ or $R_J(t,\omega)$ can be determined, since the properties of the stochastic processes are known.

A continuous distribution for the queue length imposes infinite number of constraints on the optimization on the domain Ω. Campi and Garatti (2011) provide a reformulation method for a chance-constrained optimization problem into its sample-based counterpart. A continuous stochastic event can be replaced with a finite sample of independent instances $\omega^{(1)},\ \omega^{(2)},\ldots,\omega^{(M)} \in \Omega$, distributed according to $\mathbb{P}$ where Ω is the sample-space. The optimization is then solved for M chance-constraints and the additional non-chance-constraints for every discrete time step k. In addition, Campi and Garatti (2011) studies the effect of constraint removal: what is the trade-off between performance (cost value) and constraint violation (feasibility) if m constraints are removed. Sample-based problems are solved via Monte-Carlo simulations by varying the probability level based on the distribution function (Campi et al., 2009). Monte-Carlo simulation is used as a tool for analysis: a probability level is sought where the predicted trajectory remains feasible without the control being too conservative. Feasibility means the existence of a control input that satisfies all the constraints of the optimization (Stephen Boyd, 2019).

Next, the probability sampling and discarding approach in Campi and Garatti (2011) is translated into the problem of stochastic queue lengths in the trajectory optimization. The continuous stochastic shockwave profile model in Section 2 has a natural discretization. Queue length discretization is done by discretizing the vehicle arrival rate $Q_A(t,\ \omega)$ according to $F_{Q_A}(t,\varphi)$ (i.e. discrete number of vehicles). Then, the continuous $R_J t,\ \omega$, $R_C t,\ \omega$ regions turn into discrete ones denoted by $\hat{R}_J t,\omega$, $\hat{R}_C t,\omega$ respectively.

Remark. The spatially discretized traffic flow state regions $\hat{R}_J(t,\ \omega)$ and $\hat{R}_C(t,\ \omega)$ impose finite number of nonlinear constraints on the optimization through fixed probability levels for every prediction step.

Finally, the chance-constrained optimization can be written as follows:

$$\min_{\underline{\mathbf{u}}} \left[\frac{1}{2}\underline{\mathbf{u}}^T \Phi \underline{\mathbf{u}} + \Omega^T \underline{\mathbf{u}}\right], \tag{33}$$

subject to:

$$v_{min} \le v_{des}(k) \le v_{max}, \tag{34}$$

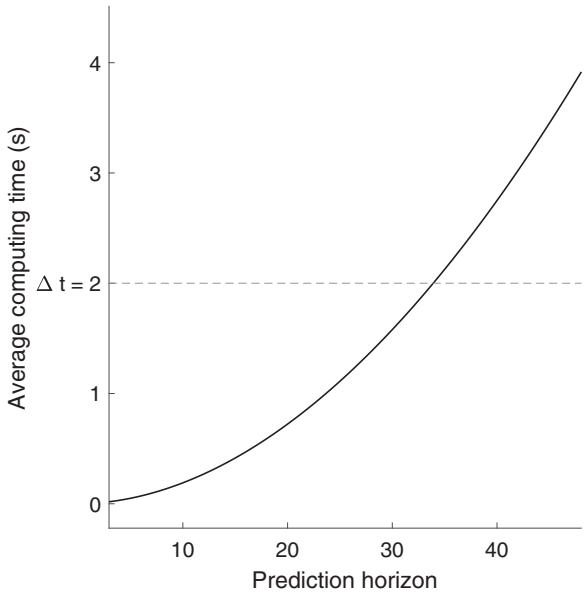

Fig. 6. Optimization time.

$$|z_{tt}(k+N|k)| < \varepsilon, \tag{35}$$

$$|v(k+N|k)| = 0, \tag{36}$$

$$v(k+i|k) = v_J = 0,\ if\ x(k+i|k) \in \hat{R}_J(t,\ \omega),\ \forall i = 1.N, \tag{37}$$

$$v(k+i|k) = v_c,\ if\ x(k+i|k) \in \hat{R}_C(t,\ \omega),\ \forall i = 1.N. \tag{38}$$

The objective function is quadratic and the constraints are nonlinear. This leads to a non-convex problem which is solved with sequential quadratic programming (SQP). Furthermore, due to the varying horizon length N, computational demand can vary. The speed of the optimization is evaluated with increasing prediction horizon length (i.e. increasing number of equations to solve). The step time length of the discrete model is $\Delta t = 2\ s$. It is desired to solve the problem under this value. According to Fig. 6 the algorithm can predict one minute ahead in real-time. Note that dedicated embedded hardware can perform such calculations faster.

The stochasticity in the constraints will inevitably propagate to the solution of the minimization problem (i.e. the predicted trajectory). Although the stochastic properties of the constraints are known, the explicit connection of stochastic properties between the constraints and the solution fades away. In the following section this connection is interpreted via numerical simulations by varying queue constraints for accurate prediction.

5. Simulations

The proposed model predictive controller is analyzed from two aspects. First, feasibility of the predicted trajectories from a deterministic starting point is studied. Second, based on a microscopic traffic simulator the proposed chance-constrained optimal velocity control is compared to other benchmark strategies.

5.1. Feasibility study

The goal of this analysis is finding a probabilistic measure to quantify the validity of the result. A confidence level is sought where the predicted trajectory remains feasible without the control being too conservative.

The bus predicts its trajectory towards the next stop from a given deterministic initial condition. There are three traffic lights between the bus and the next stop. The signal timings and traffic flow rates upstream each traffic light is summarized in Table 2.

Table 2
Signal program and vehicle flow upstream each traffic light.

Light ID	Location $l_l\,(m)$	Cycle time $t_{cyc}\,(s)$	Green time $t_{green}\,(s)$	Switch time $t_1\,(s)$	Mean arrival rate $\mathcal{Q}_A\,(veh/h)$
#1	220	60	40	50	550
#2	370	100	40	0	550
#3	470	60	40	10	550

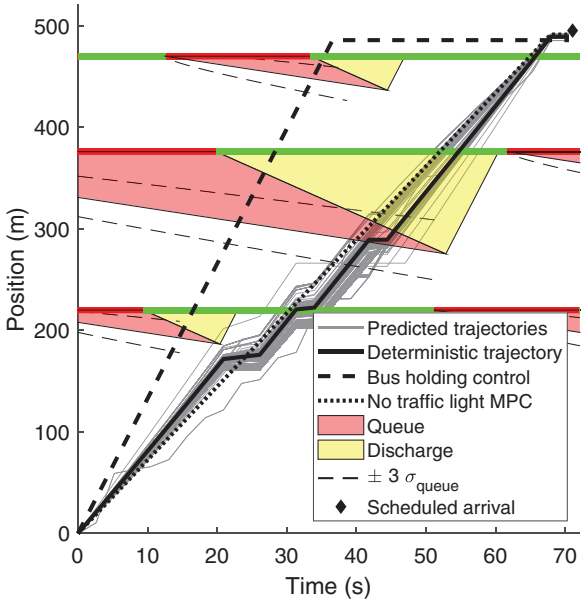

Fig. 7. Trajectory prediction distribution. Red areas indicate jam regions $R_J(t,\omega)$, yellow areas indicate queue discharge regions $R_C(t,\omega)$. Dashed lines at the shockwave profiles indicate the queue length distribution with $\pm 3\sigma_{queue}$. (For interpretation of the references to colour in this figure legend, the reader is referred to the web version of this article.)

The experimental network layout is as follows. The distance from the next stop is $500\,m$ and the target arrival time is $70\,s$. Assuming $\Delta t = 2\ s$ this results in $N = 35$.

The aim of this simulation is evaluating predicted trajectories when queue lengths are randomly generated in a Monte Carlo simulation. That is, the inflow volumes $Q_A(t,\omega)$ are randomly chosen from their distribution function $F_{Q_A}(t,\varphi)$. To keep the demonstration simple, vehicle inflows to the network follow independent Poisson distributions with constant (time-independent) arrival rate 2. By varying the magnitude of the input traffic volumes, shockwave profiles and traffic state regions change too. The regions $\hat{R}_J(t,\omega)$ and $\hat{R}_J(t,\omega)$ play part in the trajectory prediction as chance constraints. Fig. 7 presents the set of predicted trajectories in the Monte Carlo simulation (with 1000 runs). The planned trajectories arrive at the desired position by the end of the prediction with some tolerance. The predicted desired velocities are zero at the jam region and vehicles arrive at the destination on time, obeying the constraints imposed by the SPM. According to Fig. 7, the vehicles would slow down and wait upstream the queue and only enter it for a short time, resulting in somewhat counter-intuitive trajectory shapes. Despite being counter-intuitive, the solutions are feasible, since there are infinitely many feasible solutions. Note that, due to the sparse sampling ($\Delta t = 2\ s$) it is possible that the predicted trajectory does not stop exactly upon arriving at a queue but slightly after. Furthermore, Fig. 7 also presents two trajectories: bus holding and an MPC that does not consider traffic lights, thus they violate constraints.

As a metric for analysis, the spatial standard deviations are calculated at every time instance and shown in Fig. 8. The prediction horizon is split in three intervals depending on the predicted position of the bus relative to traffic lights. In time interval $0-32\ s$ the standard deviation of the queue in front of the first traffic light, between $32-52\ s$ the standard deviation upstream the second traffic light are shown. Finally, between $52-68\ s$ there are no random events considered so the standard deviation is assumed to be 0.

According to Fig. 8 there is correlation between the queue lengths and predicted trajectories. When the standard deviation of the queue length σ_{queue} increases so does the standard deviation of the predicted trajectories $\sigma_{traj.}$ and peaks when entering the queue. The uncertainty in the queue length prediction (i.e. larger variance) amplifies the variance of the predicted trajectories too. When there is no stochastic queue (after $52\,s$) the predicted trajectories converge and their standard deviation decreases. In addition, the trajectory standard deviation starts decreasing upstream Light #2, since the queue forces the vehicles to stop. Figs. 9–10 suggest negative correlation between the queue length and the predicted tra-

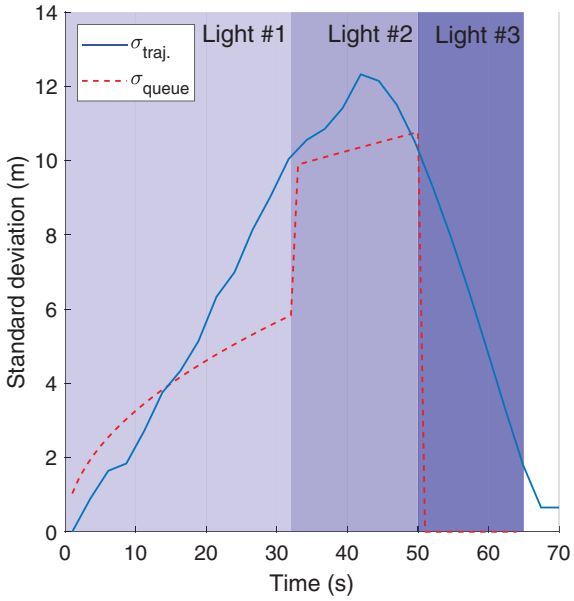

Fig. 8. Standard deviations of the queue length σ_{queue} and the predicted trajectories σ_{traj}.

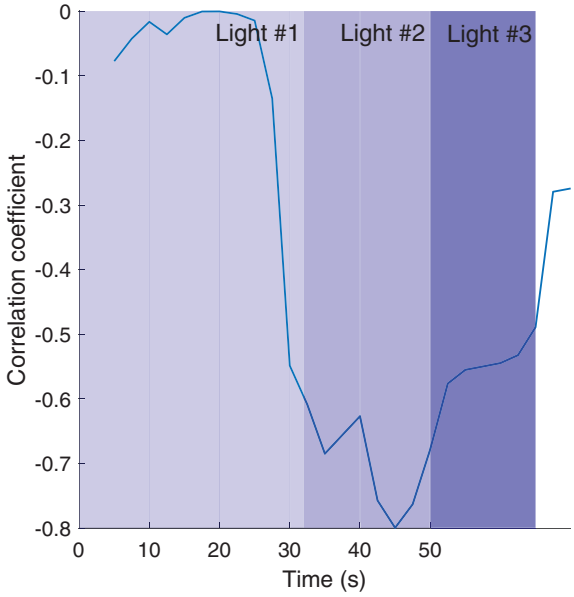

Fig. 9. Correlation coefficient between the queue lengths and the predicted trajectories over the prediction horizon.

jectory samples. Resultantly, longer queues mean the bus is farther from the desired stop, as it tries to avoid the queue and approach it slower. Next, the feasibility of the prediction is checked. Trajectories are predicted from a deterministic initial position for different probability levels. The method is translated from the sampling and discarding approach in Campi and Garatti (2011). Selecting a fixed probability level means that constraints imposed by less likely events (i.e. queue lengths) are discarded. The input flow has Poisson distribution with mean value 700 veh/h (per lane). One trajectory is predicted for confidence levels: $mean$, $mean - 2\sigma$, $mean + 2\sigma$ (Fig. 11). The prediction horizon is 50 s long and the target distance is 150 m. In the feasibility analysis it is checked if the results are feasible by calculating the relative constraint violation as follows:

$$V = \frac{1}{N}\sum_{k=1}^{N}\left|\frac{v_{des}(k) - v_{\star}(k)}{v_{des}(k)}\right|, \tag{39}$$

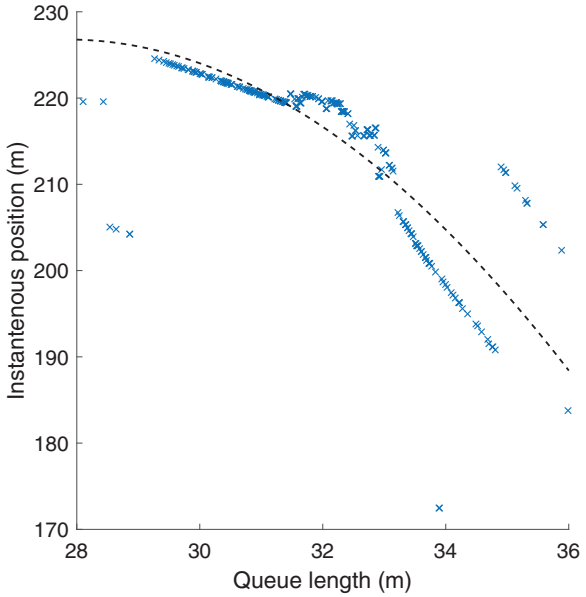

Fig. 10. Scatter plot of the queue length vs the instantaneous position samples at prediction time 35 *s*.

Table 3
Constraint violation metric *V*. Horizontal: actual arrival rate, vertical: presumed arrival rate.

Volume	647 *veh*/*h*	700 *veh*/*h*	753 *veh*/*h*
647 *veh*/*h*	0.132	0.202	0.354
700 *veh*/*h*	0.059	0.163	0.323
753 *veh*/*h*	0	0.148	0.254

Table 4
Signal program and mean traffic flow upstream each traffic light.

Light ID	Location (*m*)	Cycle time (*s*)	Green time (*s*)	Switch time (*s*)	Mean arrival rate (*veh*/*h*)
#1	406	60	40	40	1000
#2	556	60	20	45	900
#3	650	60	40	10	1000

where $v_\star(k)$ equals $v_{des}(k)$, v_J, v_C, depending on which region the k^{th} step of the predicted trajectory is in. The value of V at each test is summarized in Table 3. The constraint violation value V is not zero in the tested cases. Results in Table 3 point towards a trivial conclusion: when the actual (measured) queue length is larger than the queue length used for prediction, prediction results tend to be less feasible and vice versa. When the queue length used for prediction is larger than actual queue lengths, it would cause unnecessary stops (Figure 11). However, accounting for larger inflow rate (i.e. larger probability than the actual queue length) leads to more robust results, more room for correction along the vehicle's trajectory and more reliable bus arrivals at a stop.

Although, Table 3 suggests that predictions from a deterministic initial state are not feasible they are adequate. In the rolling horizon MPC scheme only the first step of the prediction is used. Simulation results suggest that the first prediction step is feasible if the constraints are not too restrictive for the trajectory planning.

5.2. Microscopic traffic simulation

In the followings, the proposed trajectory planning is tested in a microscopic traffic simulator VISSIM (PTV, 2011). The simulation scenario is a slightly modified version of that used in the Monte Carlo simulation. The queue lengths are estimated with 70%, i.e. the queue lengths will be overestimated for guaranteed avoidance of stopping. The model is based on a real route section in Budapest's XI^{th} district, see Fig. 12. The route section is 1 *km* long and has two bus stops with three traffic lights in between. Signal programs and mean traffic flow volume in front of each traffic light is summarized in Table 4. The route has two lanes, no dedicated lanes and fixed-time signal program. The legal speed limit is 50 km/h on the whole route. The time headway of the buses is 3 minutes. The proposed MPC algorithm is compared to three benchmark controllers:

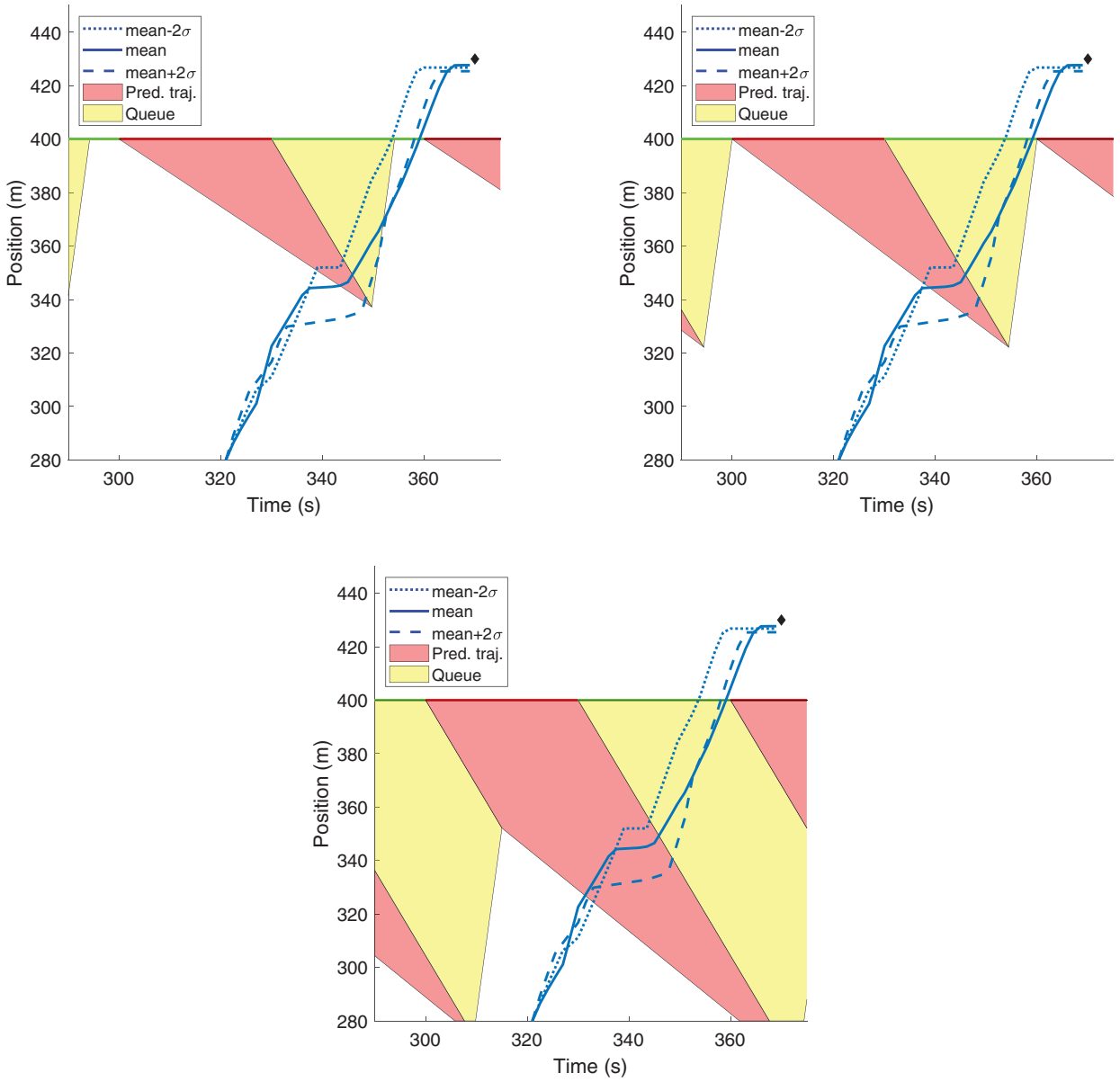

Fig. 11. Predicted trajectories for -2σ (dotted line) - 700 (solid line) - $+2\sigma$ (dashed line) *veh*/*h* compared to the SPM at 647 ($mean - 2\sigma$) (top left) - 700 (top right) - 753 ($mean + 2\sigma$) (bottom) *veh*/*h*.

i) bus holding strategy,
ii) an MPC with only traffic signal state information, and
iii) an MPC that does not consider traffic lights at all.

The trajectories generated by the four control strategies in space-time diagram are presented in Fig. 13.

The holding strategy is greedy, as the set desired velocity for buses between bus stops is 50 km/h, thus they try to get to the next stop as fast as possible. At stops, they wait until their scheduled departure time. Compared to other strategies there are steeper decelerations and accelerations when entering or leaving queues, respectively. Steep accelerations decrease ride comfort and increase energy consumption. In addition, buses following this strategy are more likely to be held in queues for longer times. When not considering traffic lights at all, buses go slower and may miss the green traffic light window where it has to cross the intersection in order to arrive on time. Therefore, for an urban velocity control strategy to work, it is crucial to take into account upstream obstacles, such as traffic lights. The benchmark algorithm that operates without queue length information can hold the timetable and be faster than the proposed chance-constrained MPC. The controller assumes there are no queues at traffic lights and can cross the intersection right after the light turns green. Without assuming queues,

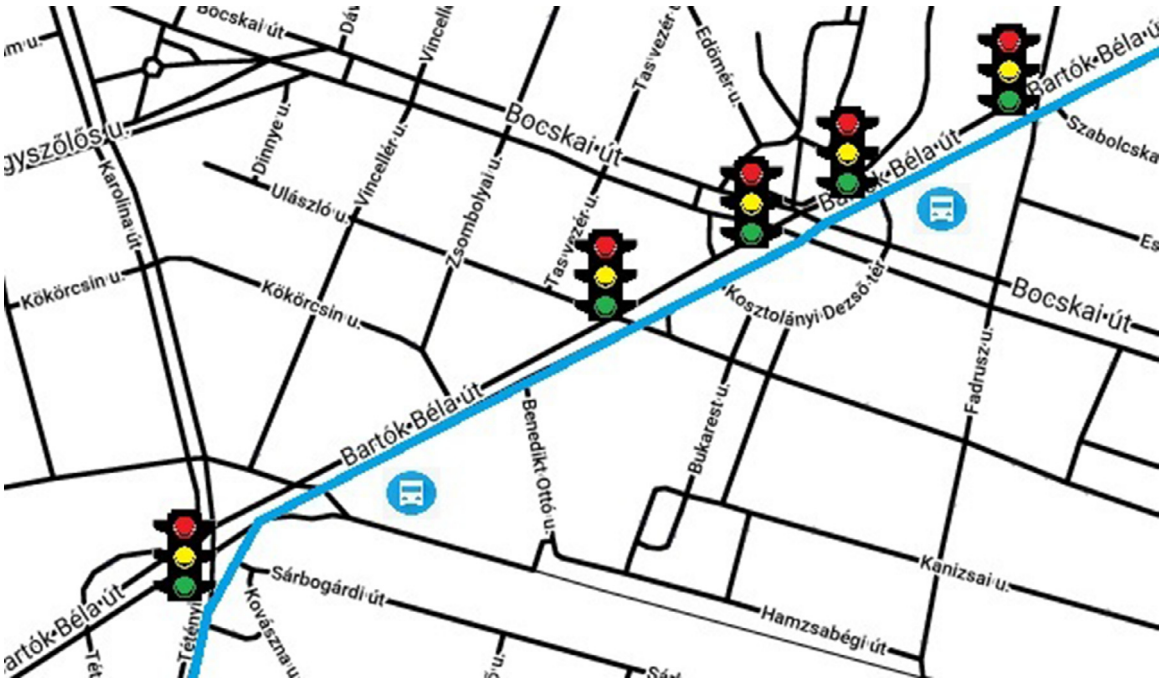

Fig. 12. Modeled route with traffic lights, Budapest XI^{th} district, GPS coordinates: 47.4754, 19.0401 (source: OpenStreetMap).

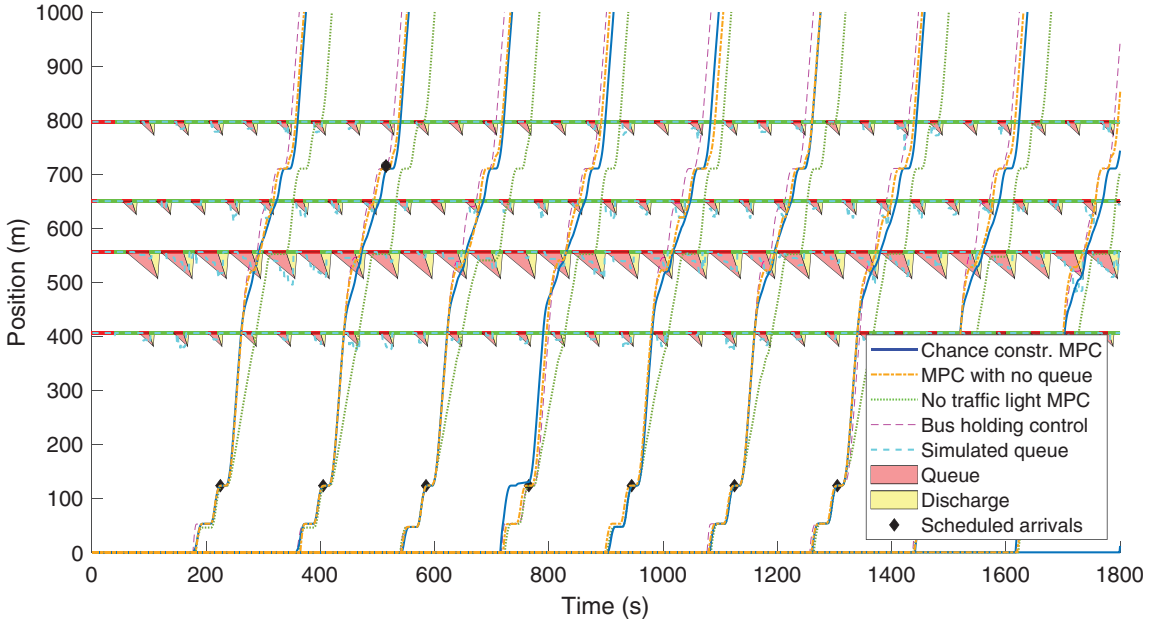

Fig. 13. Bus trajectories. A detailed section of this figure can be seen in Fig. 14.

it has to often come to a full stop at traffic lights. Finally, buses with the chance-constrained MPC take traffic light cycles and queue lengths into account and drive accordingly. Buses slow down before entering the queue or even try to elude it, avoiding coming at a full stop, saving energy (Varga et al., 2019).

In Fig. 14, at the third traffic light the measured queue is shorter than the predicted. The queue length aware bus slows down so it may avoid the predicted queue. This finding suggests that, it is not sufficient only to predict queue lengths, queue lengths shall be continuously adjusted with the actual measured queue lengths if they are available. Without proper traffic light information such velocity control algorithms may fail, as seen in the case of the “no queue MPC” or “no traffic

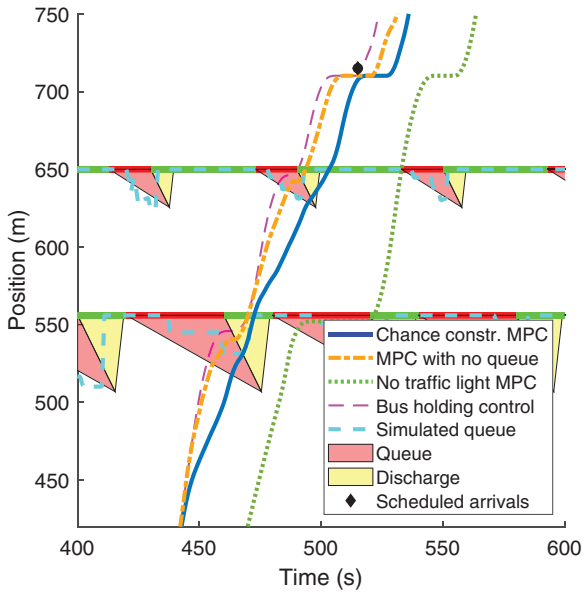

Fig. 14. Bus trajectories - zoomed.

light MPC" velocity controllers. Chance-constraints are therefore adding efficient probabilistic guarantees to velocity control algorithms.

6. Conclusions

The paper presented a velocity control algorithm for public transport buses to enhance timetable reliability in a predictive way. The proposed speed advisory system choses an optimal velocity profile towards the next bus stop. The model predictive controller incorporates real-time traffic signalization and queue lengths explicitly in the model to improve the accuracy of speed prediction. First, a traffic model, adequate to describe traffic states in front of signalized intersections - the shockwave profile model was extended with stochastic vehicle arrivals. The CDF of the shockwave profiles and the queue length are derived analytically. The model is capable of handling generic, truncated or discontinuous input distributions. Comparison against a microscopic traffic simulator suggests that the model can adequately predict queue lengths, assuming constant vehicle arrival rates.

The proposed stochastic traffic model was incorporated into a model predictive control scheme, resulting in a chance-constrained optimization. The viability of the resulting speed control algorithm was demonstrated via simulations. First, fixed initial condition simulations were performed, fixing the initial conditions and varying queue lengths in a Monte Carlo simulation. Results are feasible, however, counter-intuitive. Buses would rather not enter the queue but wait in front of it and only cross the intersection after the queue has dissipated. Second, feasibility studies were ran. It was found that results are more feasible if the controller overshoots the queue length (i.e. predicts longer queue lengths). However, the constraints are not completely satisfied, the results are still acceptable, since in the MPC scheme only the first step of the prediction is used, the rest is discarded. This means, some information about the queue lengths still propagates to the control input. Finally, the controller was compared to a greedy, bus holding control algorithm and an MPC without information about the traffic lights ahead in a microscopic traffic simulator. The proposed chance-constrained MPC controller has information about the upcoming queue it slows down earlier and may even avoid coming to a complete stop, resulting in better energy efficiency. Simulation results also suggest that in velocity control algorithms with fixed desired arrival time it is crucial to consider traffic lights as sources of delays. In addition, it is important to continuously adjust queue length predictions with the actual, measured queue lengths.

As a future research direction, three directions are envisioned. First, we plan to use generic queue length distributions with conditional probabilities, since preceding intersections and junctions perturb vehicle arrival patterns. Second, combining the controller with real-time measurements of the queue lengths can enhance the accuracy of the proposed algorithm. Third, a combined control incorporating responsive traffic lights, spillover and trajectory control will be formulated.

Declaration of Competing Interest

The authors declare that they do not have any financial or nonfinancial conflict of interests.

CRediT authorship contribution statement

Balázs Varga: Conceptualization, Methodology, Software, Formal analysis, Writing - original draft, Writing - review & editing. **Tamás Tettamanti:** Conceptualization, Methodology, Writing - review & editing. **Balázs Kulcsár:** Conceptualization, Methodology, Writing - review & editing, Supervision. **Xiaobo Qu:** Writing - review & editing, Supervision.

Acknowledgements

The research reported in this paper was supported by the Higher Education Excellence Program in the frame of Artificial Intelligence research area of Budapest University of Technology and Economics (BME FIKP-MI/FM). The authors acknowledge the contribution of Transport Area of Advance at Chalmers University of Technology. The project has been partially supported by Energimyndigheten through the project “Operational Network Energy Management for Electrified buses”.

Appendix A. Network SPM

The stochastic SPM can be further extended to handle more than a single link for queue length estimation, by taking into consideration the adjacent links, i.e. a traffic network can be modeled by SPM. Throughout the paper, unconditional distribution for traffic inflow $Q_A(t, \omega)$ was assumed. The SPM model can recursively applied for upstream links. This assumes that the inflows (and their respective CDF) in the perimeter of the network are known.

First, determine the stochastic process for the inflow $Q_A(t, \omega)$ to link A for the network in Fig. A.15. The number of outflowing vehicles from a link per traffic light cycle can be computed with the help of Eq. (13) in Section 2.3. The computed outflow $n(c, \omega)$ can be scaled up with the help of cycle times t_{cyc} to compute the total outflow $Q_B(t, \omega)$ for link B and so on. Next, assume the turning rates $\alpha_B, \alpha_C, \alpha_D$ at every intersection are known. This is a common, practical assumption for network-level traffic models (e.g. Aboudolas et al. (2009), Lin et al. (2010)). Then, the stochastic process for $Q_A(t, \omega)$ can be given as:

$$Q_A(t, \omega) = Q_B(t, \omega)\alpha_B + Q_C(t, \omega)\alpha_C + Q_D(t, \omega)\alpha_D. \tag{A.1}$$

Next, the method for obtaining the CDF of the inflow $F_{Q_A}(t, \varphi)$ is given. If the inflows $Q_B(t, \omega), Q_C(t, \omega), Q_D(t, \omega)$ are independent,

$$F_{Q_A}(t, \varphi) = F_{Q_B}(t, \varphi_B) * F_{Q_C}(t, \varphi_C) * F_{Q_D}(t, \varphi_D) \tag{A.2}$$

as convolution is an associative operation. If the flows are not independent, their joint probability shall be known (Arnold, 2013).

After obtaining $Q_A(t, \omega)$ and $F_{Q_A}(t, \omega)$ from the aforementioned steps, the computation of traffic states and queue lengths in a probabilistic sense can be performed as described in Section 2.4.

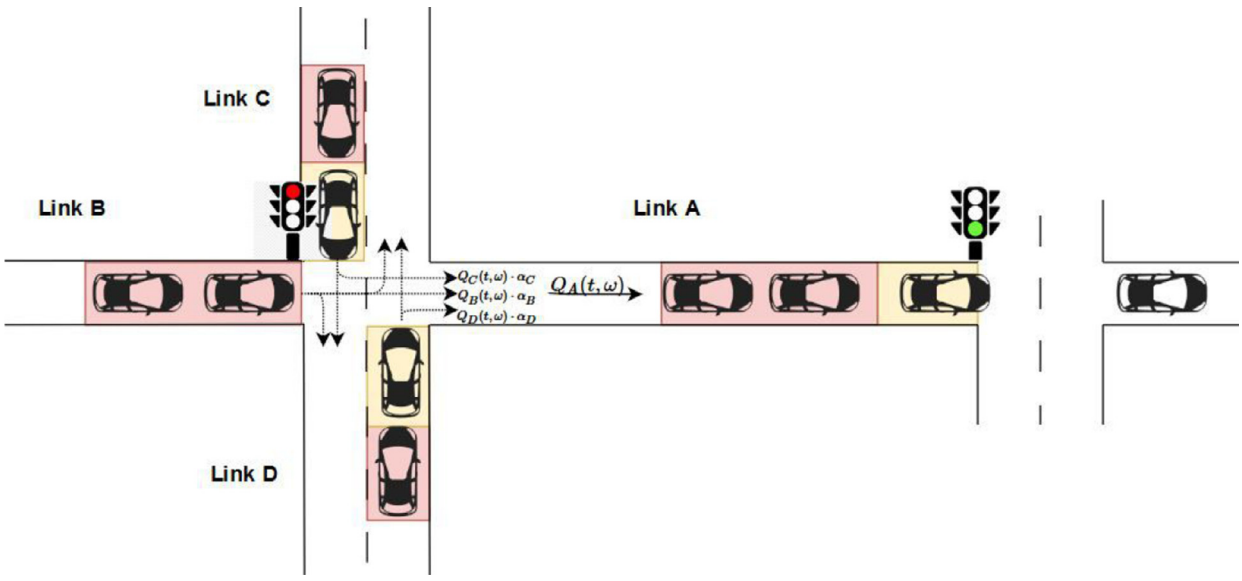

Fig. A.15. Shockwave profile model based queues at on network level.

In an urban network, in case of heavy congestion, blocking or queue spillover can occur. Similarly to Chow et al. (2015), it is handled by bounding the queue length on a given link:

$$\hat{l}_q(t,\omega) = min(l_q(t,\omega), L_A), \tag{A.3}$$

where L_A is the length of *Link A*, defined between two intersections.

Supplementary material

Supplementary material associated with this article can be found, in the online version, at doi:10.1016/j.trb.2020.06.005.

References

Aboudolas, K., Papageorgiou, M., Kosmatopoulos, E., 2009. Store-and-forward based methods for the signal control problem in large-scale congested urban road networks. Transportation Research Part C: Emerging Technologies 17 (2), 163–174. doi:10.1016/j.trc.2008.10.002.

Akhegaonkar, S., Nouveliere, L., Glaser, S., Holzmann, F., 2018. Smart and green ACC: energy and safety optimization strategies for EVs. IEEE Transactions on Systems, Man, and Cybernetics: Systems 48 (1), 142–153. doi:10.1109/TSMC.2016.2600273.

Arnold, L., 2013. Random dynamical systems. Springer Science & Business Media doi:10.1007/978-3-662-12878-7.

Campi, M.C., Garatti, S., 2011. A sampling-and-discarding approach to chance-constrained optimization: feasibility and optimality. J. Optim. Theory Appl. 148 (2), 257–280. doi:10.1007/s10957-010-9754-.

Campi, M.C., Garatti, S., Prandini, M., 2009. The scenario approach for systems and control design. Annu. Rev. Control 33 (2), 149–157.

Chiabaut, N., Buisson, C., Leclercq, L., 2009. Fundamental diagram estimation through passing rate measurements in congestion. IEEE Trans. Intell. Transp. Syst. 10 (2), 355–359. doi:10.1109/TITS.2009.2018963.

Chow, A.H., Li, S., Szeto, W., Wang, D.Z., 2015. Modelling urban traffic dynamics based upon the variational formulation of kinematic waves. Transportmetrica B: Transport Dynamics 3 (3), 169–191. doi:10.1080/21680566.2015.1005559.

Chow, A.H., Li, S., Zhong, R., 2017. Multi-objective optimal control formulations for bus service reliability with traffic signals. Transportation Research Part B: Methodological 103, 248–268. doi:10.1016/j.trb.2017.02.006.

Comert, G., Cetin, M., 2009. Queue length estimation from probe vehicle location and the impacts of sample size. Eur. J. Oper. Res. 197 (1), 196–202. doi:10.1016/j.ejor.2008.06.024.

Daganzo, C.F., 2009. A headway-based approach to eliminate bus bunching: systematic analysis and comparisons. Transportation Research Part B: Methodological 43 (10), 913–921. doi:10.1016/j.trb.2009.04.002.

Daganzo, C.F., Lehe, L.J., 2016. Traffic flow on signalized streets. Transportation Research Part B: Methodological 90, 56–69. doi:10.1016/j.trb.2016.03.010.

Dakic, I., Ambhl, L., Schmperlin, O., Menendez, M., 2019. On the modeling of passenger mobility for stochastic bi-modal urban corridors. Transportation Research Part C: Emerging Technologies doi:10.1016/j.trc.2019.05.018.

Darroch, J., 1964. On the traffic-light queue. The Annals of Mathematical Statistics 35 (1), 380–388. doi:10.1214/aoms/1177703761.

Fathy, M., Siyal, M., 1998. A window-based image processing technique for quantitative and qualitative analysis of road traffic parameters. IEEE Trans. Veh. Technol. 47 (4), 1342–1349. doi:10.1109/25.728525.

Gu, W., Cassidy, M.J., Gayah, V.V., Ouyang, Y., 2013. Mitigating negative impacts of near-side bus stops on cars. Transportation Research Part B: Methodological 47, 42–56. doi:10.1016/j.trb.2012.09.005.

Guler, S.I., Menendez, M., 2014. Analytical formulation and empirical evaluation of pre-signals for bus priority. Transportation Research Part B: Methodological 64, 41–53. doi:10.1016/j.trb.2014.03.004.

Heidemann, D., 1994. Queue length and delay distributions at traffic signals. Transportation Research Part B: Methodological 28 (5), 377–389. doi:10.1016/0191-2615(94)90036-1.

Helbing, D., Tilch, B., 1998. Generalized force model of traffic dynamics. Physical review E 58 (1), 133. doi:10.1103/PhysRevE.58.133.

Hellström, E., Åslund, J., Nielsen, L., 2010. Design of an efficient algorithm for fuel-optimal look-ahead control. Control Eng. Pract. 18 (11), 1318–1327. doi:10.1016/j.conengprac.2009.12.008.

Karlin, S., 1957. A first course in stochastic processes, 2 Academic Press doi:10.1016/C2009-1-28569-8.

Klumpenhouwer, W., Wirasinghe, S., 2018. Optimal time point configuration of a bus route-a markovian approach. Transportation Research Part B: Methodological 117, 209–227. doi:10.1016/j.trb.2018.08.021.

Kural, E., Jones, S., Parrilla, A.F., Grauers, A., 2014. Traffic light assistant system for optimized energy consumption in an electric vehicle. In: International Conference on Connected Vehicles and Expo (ICCVE). IEEE, 3–7 November, 2014, Vienna, Austria, pp. 604–611. doi:10.1109/ICCVE.2014.7297619.

Laval, J.A., Castrillón, F., 2015. Stochastic approximations for the macroscopic fundamental diagram of urban networks. Transp. Res. Procedia 7, 615–630. doi:10.1016/j.trpro.2015.06.032.

Li, X., Ghiasi, A., Xu, Z., Qu, X., 2018. A piecewise trajectory optimization model for connected automated vehicles: exact optimization algorithm and queue propagation analysis. Transportation Research Part B: Methodological 118, 429–456. doi:10.1016/j.trb.2018.11.002.

Lin, S., Schutter, B.D., Xi, Y., Hellendoorn, H., 2010. Model predictive control for urban traffic networks via MILP. In: Proceedings of the 2010 American Control Conference. IEEE doi:10.1109/acc.2010.5530534.

Liu, H.X., Wu, X., Ma, W., Hu, H., 2009. Real-time queue length estimation for congested signalized intersections. Transportation Research Part C: Emerging Technologies 17 (4), 412–427. doi:10.1016/j.trc.2009.02.003.

Maciejowski, J.M., 2002. Predictive control: With constraints, 1st Prentice Hall, Harlow, UK.

Mung, G.K., Poon, A.C., Lam, W.H., 1996. Distributions of queue lengths at fixed time traffic signals. Transportation Research Part B: Methodological 30 (6), 421–439. doi:10.1016/0191-2615(96)00009-4.

Muñoz, J.C., Daganzo, C.F., 2002. Moving Bottlenecks: A Theory Grounded on Experimental Observation. In: Transportation and Traffic Theory in the 21st Century. Emerald Group Publishing Limited, pp. 441–461. doi:10.1108/9780585474601-022.

Németh, B., Gáspár, P., 2011. Road inclinations in the design of lpv-based adaptive cruise control. IFAC Proceedings Volumes 44 (1), 2202–2207. doi:10.3182/20110828-6-IT-1002.00932.

Papageorgiou, M., 1998. Some remarks on macroscopic traffic flow modelling. Transportation Research Part A: Policy and Practice 32 (5), 323–329. doi:10.1016/S0965-8564(97)00048-7.

Park, S., Rakha, H., Ahn, K., Moran, K., 2011. Predictive eco-cruise control: Algorithm and potential benefits. In: IEEE Forum on Integrated and Sustainable Transportation Systems. IEEE, 29 June - 1 July 2011, Vienna, Austria, pp. 394–399. doi:10.1109/FISTS.2011.5973639.

PTV, 2011. VISSIM 5.30-05 User Manual. PTV. Stumpfstrasse 1, D-76131 Karlsruhe, Germany.

Qu, X., Wang, S., Zhang, J., 2015. On the fundamental diagram for freeway traffic: anovel calibration approach for single-regime models. Transportation Research Part B: Methodological 73, 91–102. doi:10.1016/j.trb.2015.01.001.

Qu, X., Yu, Y., Zhou, M., Lin, C.-T., Wang, X., 2020. Jointly dampening traffic oscillations and improving energy consumption with electric, connected and automated vehicles: areinforcement learning based approach. Appl. Energy 257, 114030. doi:10.1016/j.apenergy.2019.114030.

Qu, X., Zhang, J., Wang, S., 2017. On the stochastic fundamental diagram for freeway traffic: model development, analytical properties, validation, and extensive applications. Transportation Research Part B: Methodological 104, 256–271. doi:10.1016/j.trb.2017.07.003.

Saerens, B., Rakha, H.A., Diehl, M., Van den Bulck, E., 2013. A methodology for assessing eco-cruise control for passenger vehicles. Transportation Research Part D: Transport and Environment 19, 20–27. doi:10.1016/j.trd.2012.12.001.
Saif, M.A., Zefreh, M.M., Török, A., 2019. Public transport accessibility: a literature review. Periodica Polytechnica Transportation Engineering 47 (1), 36–43. doi:10.3311/PPtr.12072.
Sánchez-Martínez, G., Koutsopoulos, H., Wilson, N., 2016. Real-time holding control for high-frequency transit with dynamics. Transportation Research Part B: Methodological 83, 1–19. doi:10.1016/j.trb.2015.11.013.
Seo, T., Kawasaki, Y., Kusakabe, T., Asakura, Y., 2019. Fundamental diagram estimation by using trajectories of probe vehicles. Transportation Research Part B: Methodological 122, 40–56. doi:10.1016/j.trb.2019.02.005.
Sharma, A., Bullock, D., Bonneson, J., 2007. Input-output and hybrid techniques for real-time prediction of delay and maximum queue length at signalized intersections. Transportation Research Record: Journal of the Transportation Research Board (2035) 69–80. doi:10.3141/2035-08.
Stephen Boyd, L.V., 2019. Convex optimization. Cambridge University Press.
Varga, B., Tettamanti, T., Kulcsár, B., 2018. Optimally combined headway and timetable reliable public transport system. Transportation Research Part C: Emerging Technologies 92, 1–26. doi:10.1016/j.trc.2018.04.016.
Varga, B., Tettamanti, T., Kulcsár, B., 2019. Energy-aware predictive control for electrified bus networks. Appl. Energy 252, 113477. doi:10.1016/j.apenergy.2019.113477.
Vreeswijk, J.D., Mahmod, M., van Arem, B., 2010. Energy efficient traffic management and control-the eCoMove approach and expected benefits. In: 13th International IEEE Conference on Intelligent Transportation Systems. IEEE, 19–22 September 2010, Funchal, Portugal, pp. 955–961. doi:10.1109/ITSC.2010.5625122.
Wu, X., Liu, H.X., 2011. A shockwave profile model for traffic flow on congested urban arterials. Transportation Research Part B: Methodological 45 (10), 1768–1786. doi:10.1016/j.trb.2011.07.013.
Yang, H., Rakha, H., Ala, M.V., 2017. Eco-cooperative adaptive cruise control at signalized intersections considering queue effects. IEEE Trans. Intell. Transp. Syst. 18 (6), 1575–1585. doi:10.1109/TITS.2016.2613740.
Yang, K., Guler, S.I., Menendez, M., 2016. Isolated intersection control for various levels of vehicle technology: conventional, connected, and automated vehicles. Transportation Research Part C: Emerging Technologies 72, 109–129. doi:10.1016/j.trc.2016.08.009.
Zheng, F., Jabari, S.E., Liu, H.X., Lin, D., 2018. Traffic state estimation using stochastic lagrangian dynamics. Transportation Research Part B: Methodological 115, 143–165. doi:10.1016/j.trb.2018.07.004.